Supporting Information

Extravasating Neutrophils Open Vascular Barrier and Improve Liposomes Delivery to Tumors

Victor A. Naumenko, Kseniya Yu. Vlasova, Anastasiia S. Garanina, Pavel A. Melnikov, Daria M. Potashnikova, Daniil A. Vishnevskiy, Stepan S. Vodopyanov, Vladimir P. Chekhonin, Maxim A. Abakumov, Alexander G. Majouga

Supplementary figures

Figure S1. Stability and biocompatibility of FL.

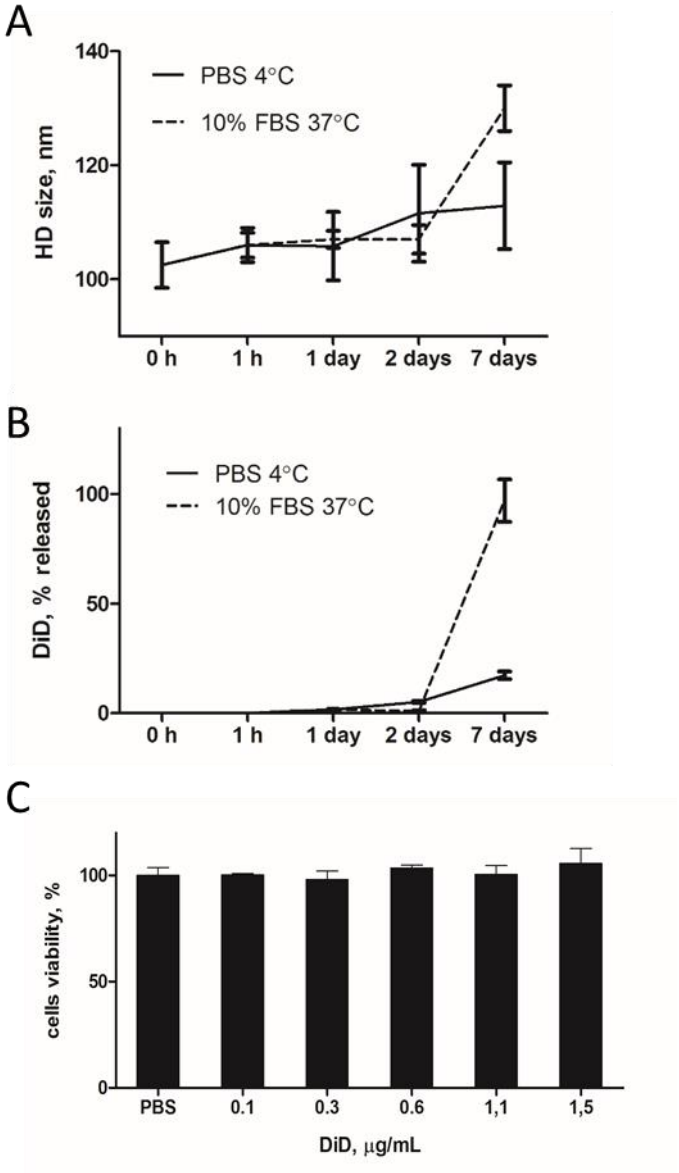

A. Dynamics of FL hydrodynamic size during 7 days incubation in 10 mM PBS (pH 7.4) at 4 ˚C (solid line) and fetal bovine serum (FBS) containing media at 37 ˚C (dashed line). **B.** Dye release from FL during 7 days incubation in 10 mM PBS (pH 7.4) at 4 ˚C (solid line) and FBS containing media at 37 ˚C (dashed line). Total lipid concentration for **A-B** was 16.8 mg/mL. **C.** FL cytotoxicity assay (MTS) on SC-1 mouse fibroblasts; 0.1-1.5 μg/mL on a DiD basis corresponds to 0.11-1.67 mg/mL lipids concentration range.

Figure S2. Biodistribution and FL accumulation in 4T1 tumors.

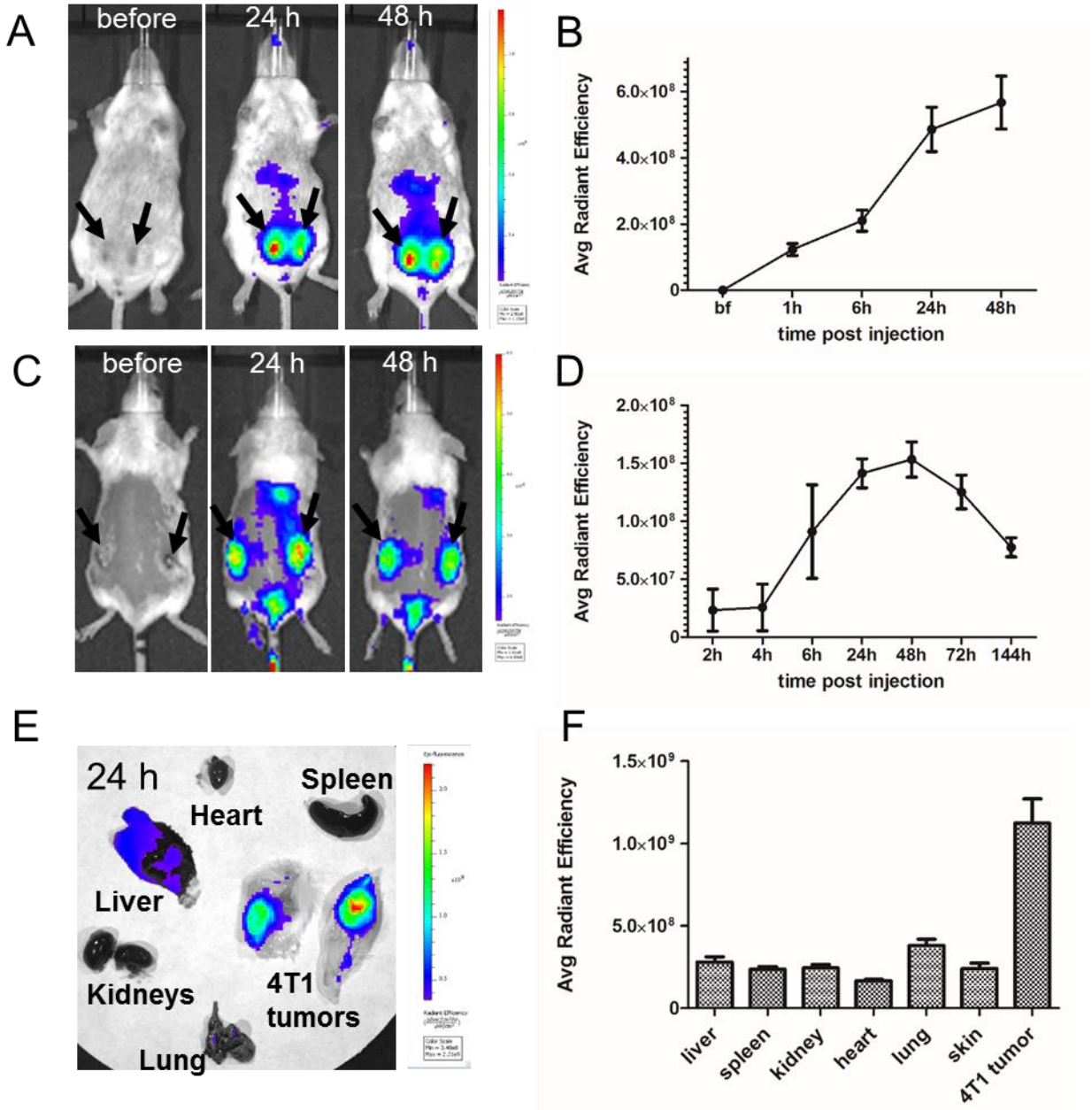

A-D. Dynamics of FL accumulation in 4T1 (OT)-tumors **(A-B)** and 4T1 (HT)-tumors **(C-D)**. **A, C.** Representative images of 4T1-bearing mice before and 24-48 h after FL (25 mg/kg) intravenous (i.v.) injection. Arrows indicate tumors. **B, D.** Quantification of fluorescence signal in 4T1 tumors upon FL injection. The data are shown as tumor signal minus signal from tumor-free skin (n=10). **E-F.** Biodistribution of FL measured *ex vivo* 24 h post injection: representative image of organs and 4T1 (HT)-tumors **(E)**, and quantification (n=3) of average radiant efficiency **(F)**. The data are shown after subtraction of background fluorescence from the corresponding organs of untreated mice (n=3).

Figure S3. Biodistribution and FL accumulation in 4T1 and 22Rv1 tumors.

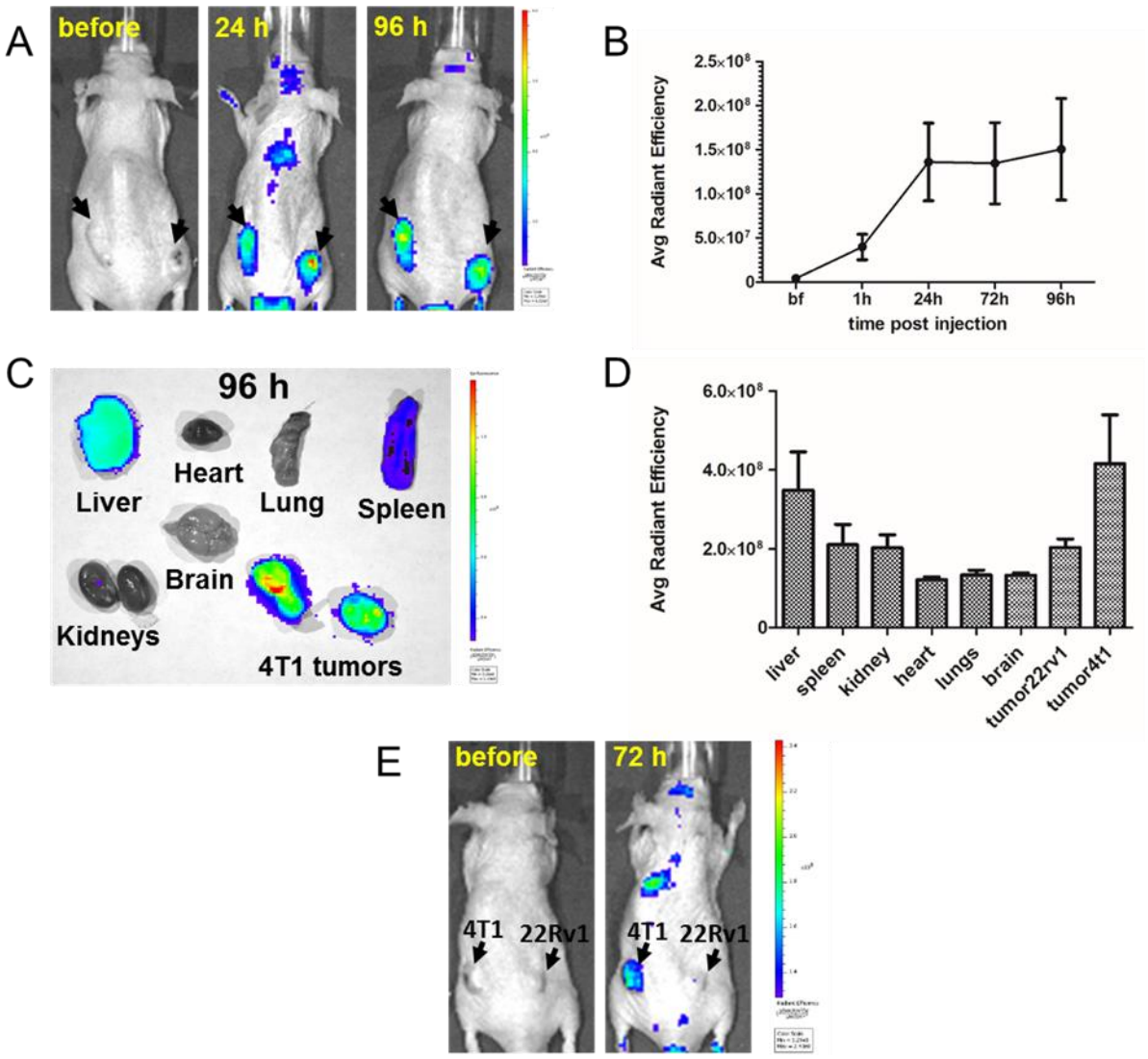

A-B. Dynamics of FL accumulation in 4T1 tumors in nude mice: representative image of animals **(A)** and quantification (n=4) of fluorescence signal before and within 96 h after FL (25 mg/kg) injection **(B)**. Arrows indicate tumors. The data are shown as tumor signal minus signal from tumor-free skin. **C-D.** Biodistribution of FL measured *ex vivo* 96 h post injection: representative image of organs and tumors **(C)**, and quantification (n=4) of average radiant efficiency **(D)**. The data are shown after subtraction of mean background fluorescence from the corresponding organs of untreated mice (n=2). **E.** Representative image of FL accumulation in 4T1 and 22Rv1 tumors implanted into contralateral flanks.

Figure S4. Colocalization of FL with neutrophils and macrophages in tissues.

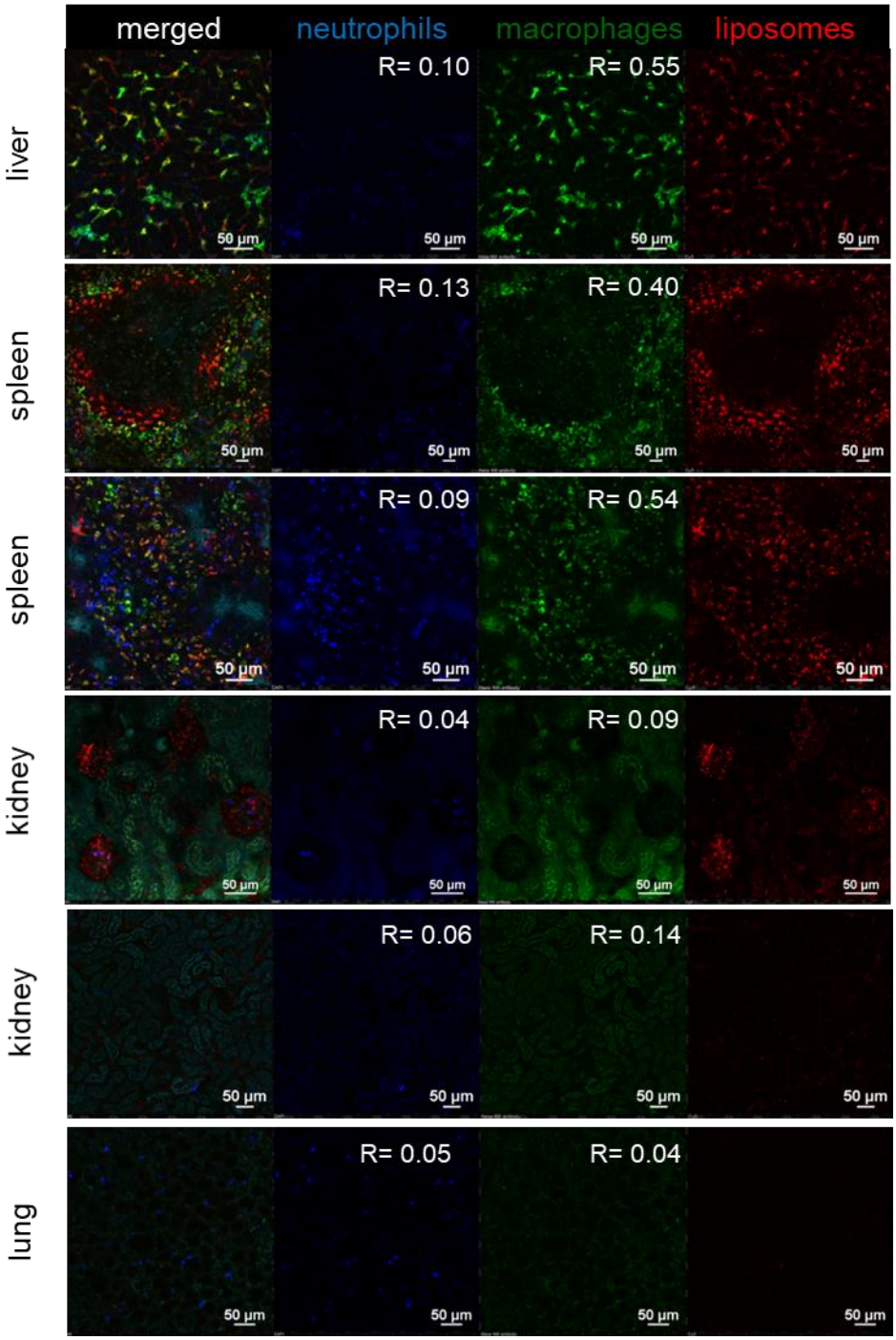

FL distribution in vital organs was studied 2 h after injection (associated with Figure 1C-H). Pearson's coefficients (R) for FL colocalization with neutrophils and macrophages markers are provided in upper right corners of corresponding panels; blue, Ly6G; green, F4/80; red, liposomes.

Figure S5. FL circulation half-lives studied by intravital microscopy (IVM).

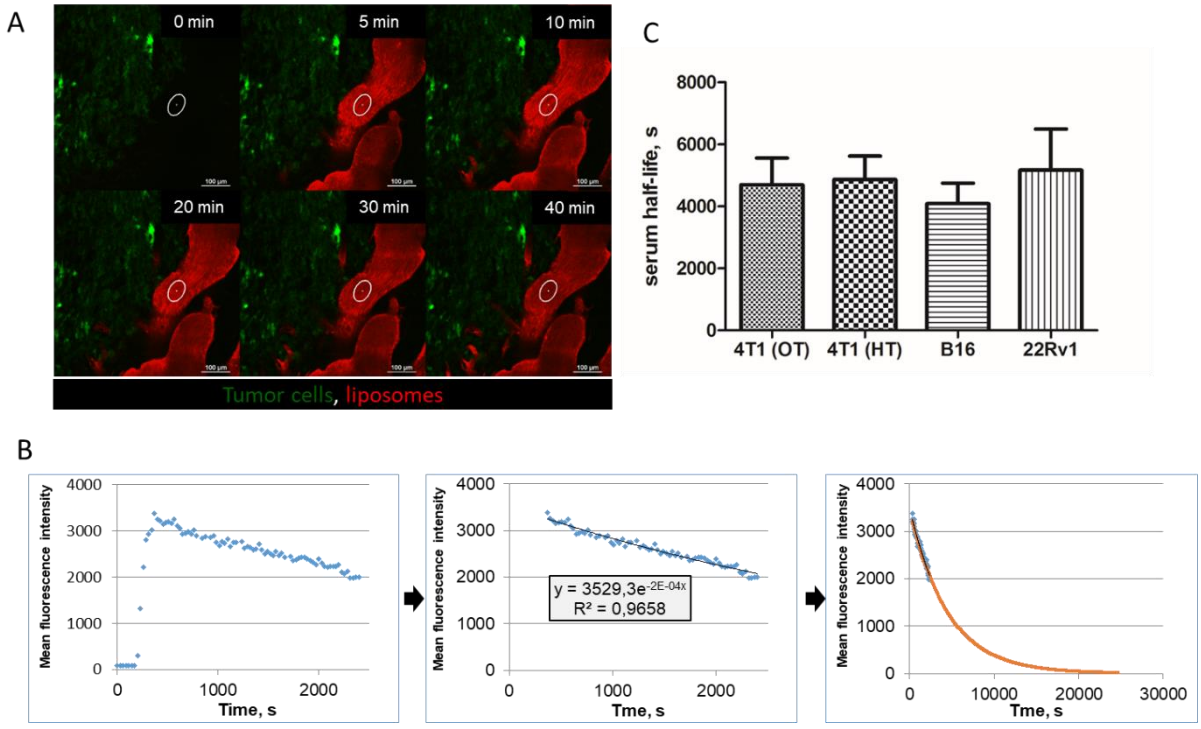

A-C. Mean fluorescence intensity was measured in the vessels during 40 min after FL injection **(A)** and plotted on graph starting from the peak fluorescence point (**B**, blue line). Using exponential function an equation for fluorescence intensity dynamics was obtained (**B**, red line) and circulation half-lives for FL in animals bearing distinct tumor types (n=3 for each group) was calculated **(C)**.

Figure S6. Characterization of dual-labeled FL.

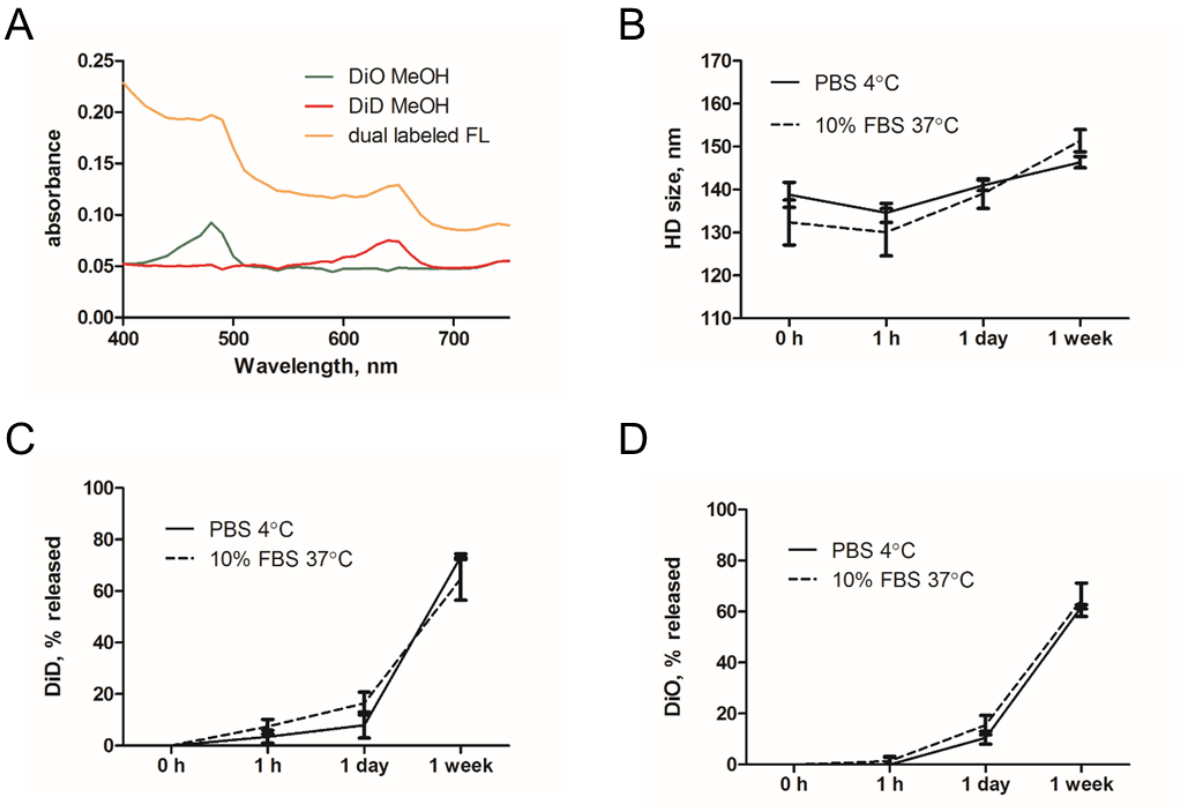

A. Absorbance spectra of DiD (0.002 µg/mL; red) and DiO (0.9 µg/mL; green) in methanol or incorporated into lipid membrane (total lipid conc. 0.2 mg/mL; orange). **B.** Dynamics of FL hydrodynamic size during 7 days incubation in 10 mM PBS (pH 7.4) at 4 ˚C (solid line) and fetal bovine serum (FBS) containing media at 37 ˚C (dashed line). **C-D.** DiD **(C)** and DiO **(D)** release from FL during 7 days incubation in 10 mM PBS (pH 7.4) at 4 ˚C (solid line) and FBS containing media at 37 ˚C (dashed line). Total lipid concentration for **B-D** was 8.4 mg/mL.

Figure S7. Colocalization of DiO and DiD signaling in dual-labeled FL.

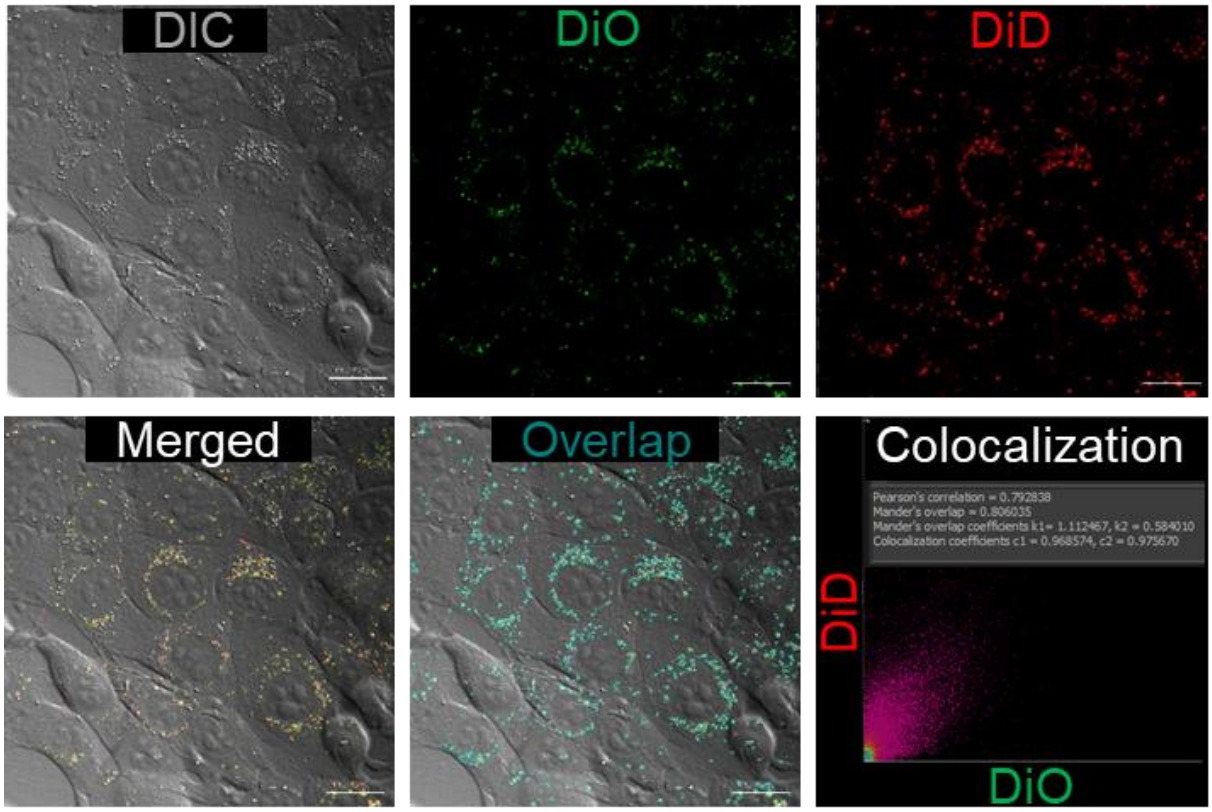

Representative image of 4T1 cells incubated with dual-labeled liposomes (50 µg/mL lipids). Cells are visualized in DIC channel. Overlapping of DiO (green) and DiD (red) is shown in cyan. High values of colocalization coefficients (c1=0.93±0.009; c2=0.93±0.02; n=10) suggest that both fluorophores are stably bound with liposomes. Scale bar, 20 µm.

Figure S8. Colocalization of DiO and DiD signaling after injecting mixture of single-labeled FL or dual-labeled FL.

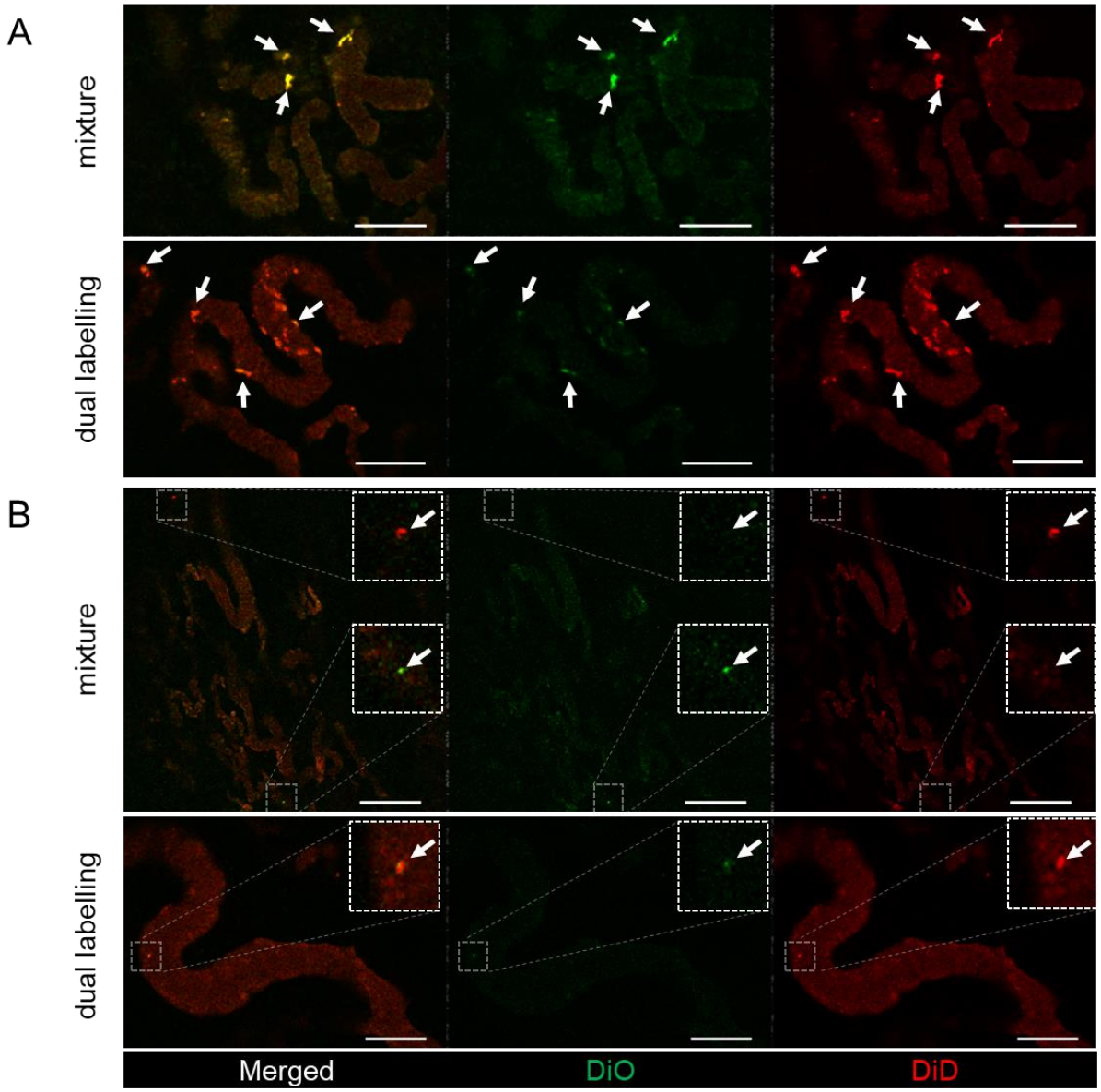

DiO- and DiD-labeled FL were premixed (50 µl + 50 µl) and i.v. injected (top panels on **A** and **B**). Alternatively, 100 µl of dual-labeled FL with the matched concentrations of DiO and DiD were administered (bottom panels on **A** and **B**). **A.** Both treatments resulted in colocalization of two labels in the blood flow and perivascular space (arrows). **B.** Circulating aggregates after injecting of dual-labeled liposomes were double positive, while the mixture of DiO- and DiD-labeled liposomes resulted in single-stained aggregates. Colocalization of DiD and DiO signals in the leakage spots and floating aggregates after injecting dual-labeled FL further supports dye stability in liposomes membrane. Scale bar, 100 µm.

Figure S9. Extravasation patterns of DiO-labeled liposomes.

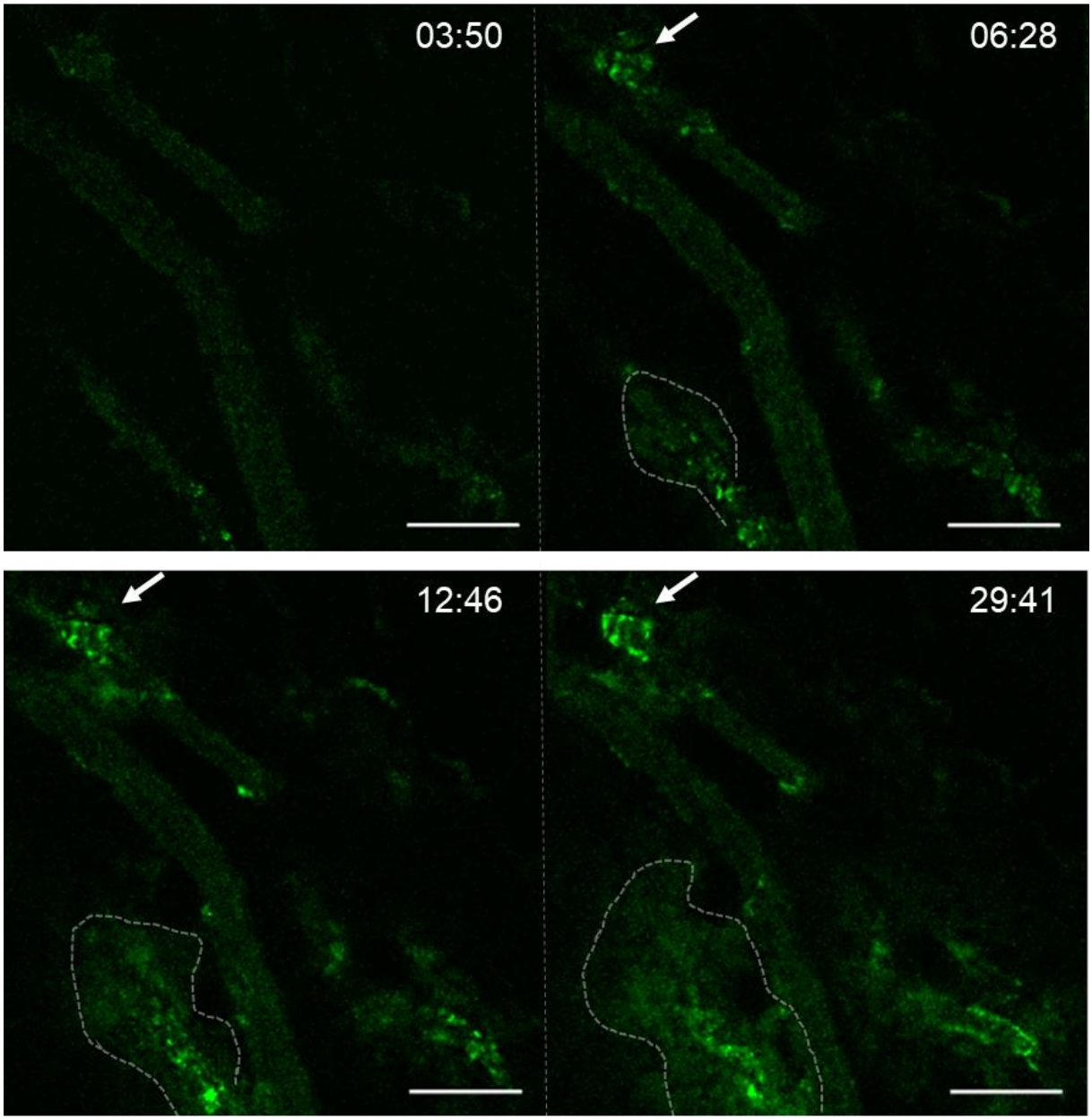

4T1-bearing mice were injected with DiO-labeled liposomes and tumor vasculature was imaged within 30 min. Microleakages (arrow) and macroleakages (dashed line) were detected similar to extravasation behavior of DiD-labeled counterparts. Scale bar, 100 μm.

Figure S10. Colocalization of FL with Doxil.

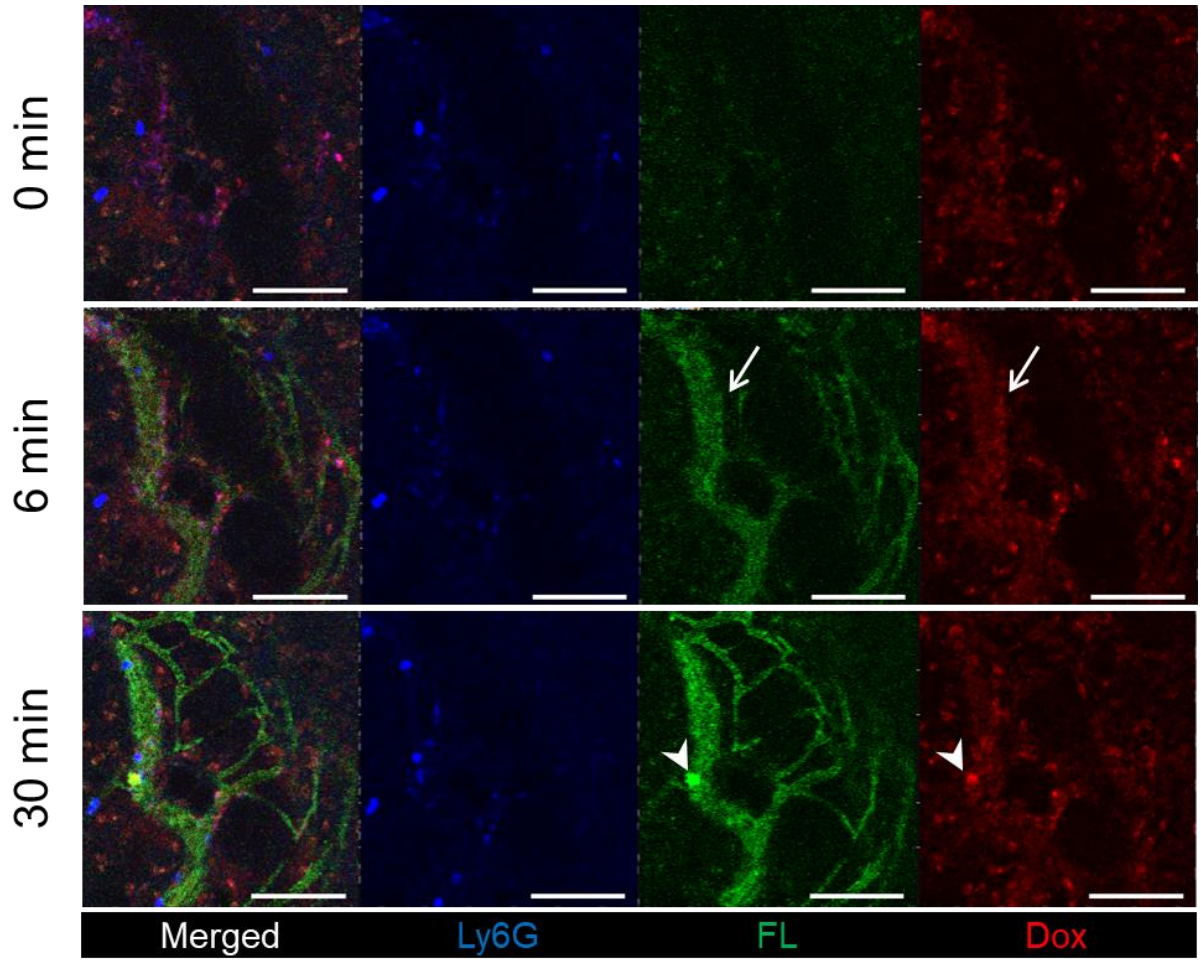

Injection of DiO-labeled liposomes (50 µl; green) was followed by injection of Doxil (Caelyx, 50 µl; red), and tumor vessels were imaged. Although Doxorubicin fluorescence intensity was suboptimal for *in vivo* imaging, we were able to see dim counterstaining of tumor vessels upon Doxil injection (arrow). More importantly, after 30 min both FL and Doxorubicin colocalized in microleakage spot (arrowhead). The results further validate liposomes extravasation patterns identified using FL. Blue, neutrophils. Scale bar, 100 µm.

Figure S11. Microleakages do not colocalize with neither leukocytes nor tumor cells.

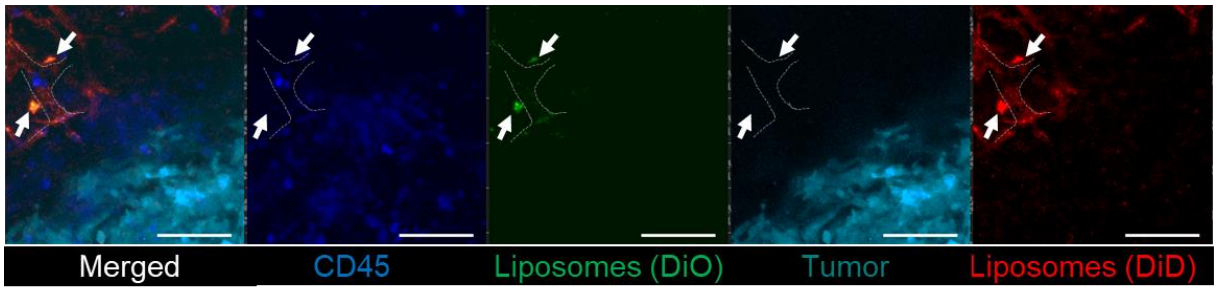

Dual-labeled liposomes (DiO, green; DiD, red) were i.v. injected while imaging 4T1 tumor cells (cyan) and leukocytes (blue). Both liposomes labels colocalized in perivascular area (arrows), but these leakage spots were negative for CD45 and tumor cells markers. Dashed lines delineate vessels. Scale bar, 100 µm.

Figure S12. Quantitative analysis of FL uptake by intravascular leukocytes.

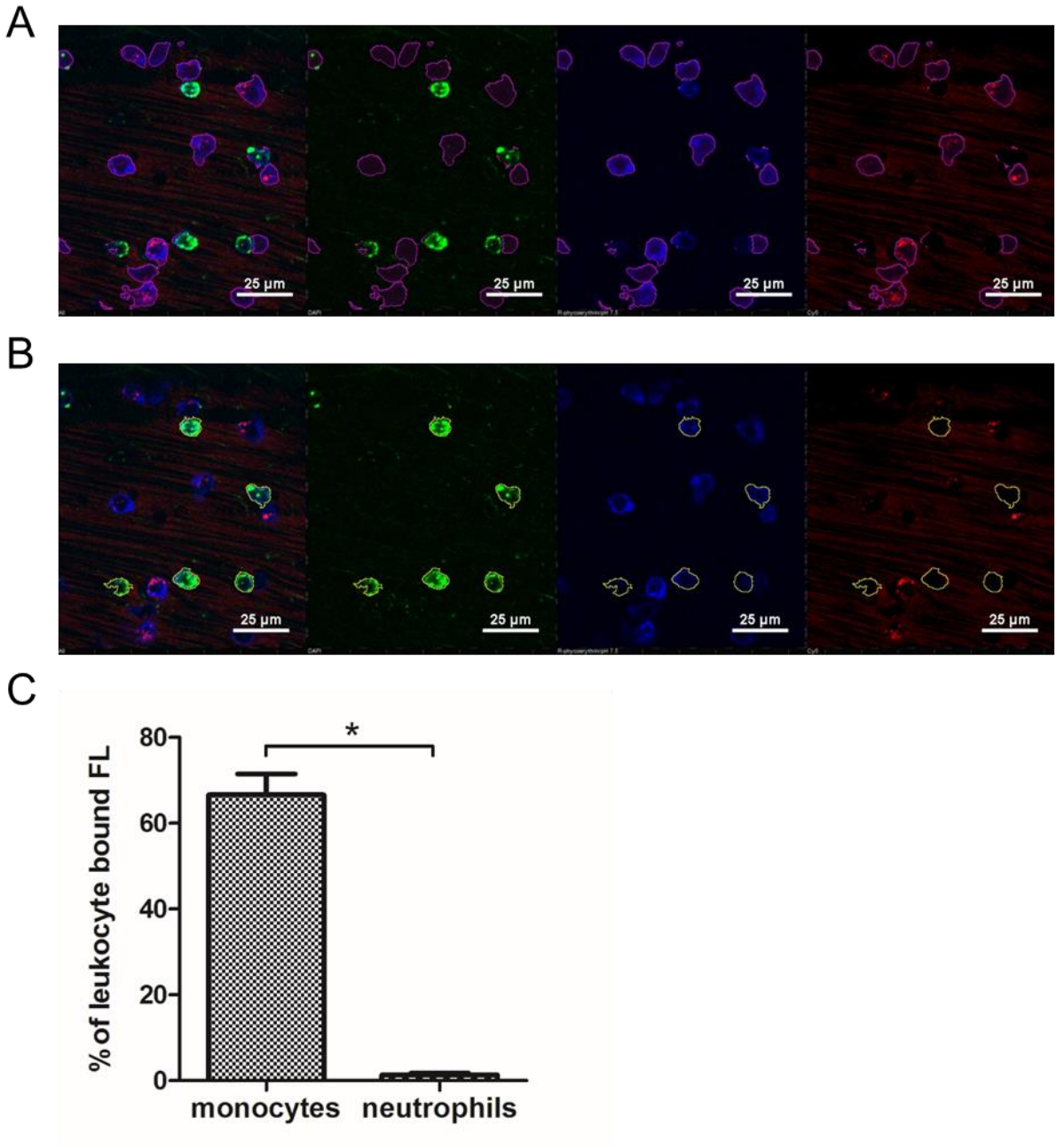

Colocalization of FL (red) with monocytes (blue) and neutrophils (green+blue) was studied in tumor vasculature (associated with Figure 5B). **A-B.** Representative examples of identifying monocytes **(A)** and neutrophils **(B)** using automatic threshold. **C.** Quantification of FL cellular uptake in monocytes- and neutrophils-associated ROI (counted in 11 FOV, approx. 200 cells), *$p<0.001$, unpaired t-test.

Figure S13. Measurements of vessel size and distance to tumor for individual leakage spot.

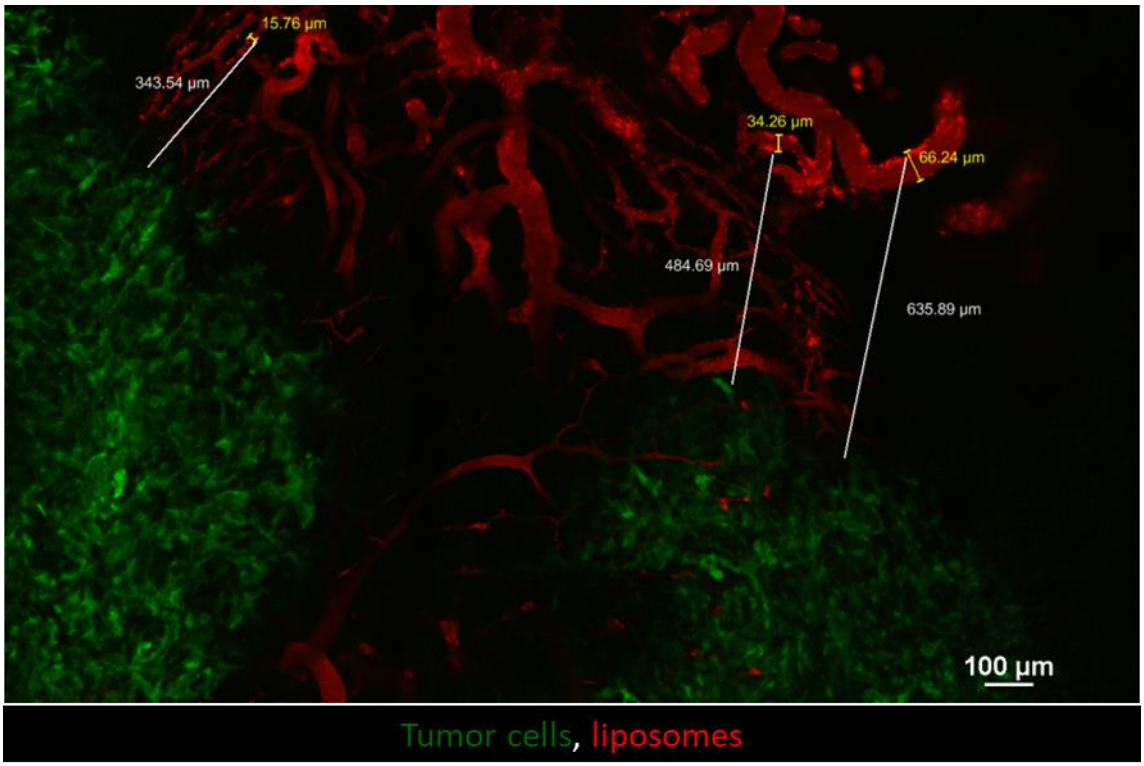

Representative example of measuring vessel diameter (yellow lines) and distance to tumor cells (white line) for three leakage spots (bright red) in 4T1-GFP tumor (green) 40 min after FL i.v. injection. Vessels are counterstained by circulating FL (red).

Figure S14. Characterization of leakages in the vessels without neutrophil infiltration.

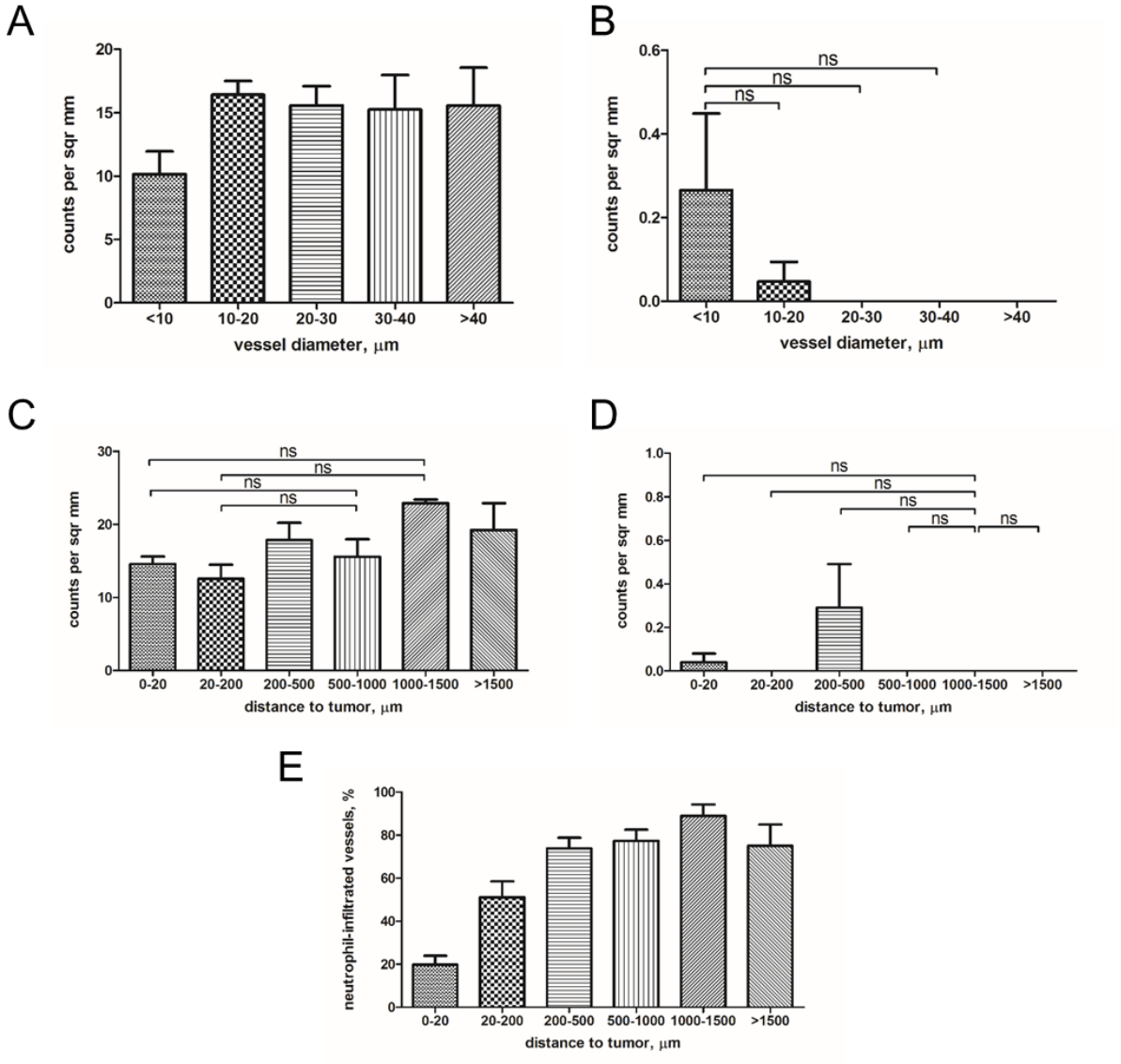

A-B. Quantification of micro- **(A)** and macroleakages **(B)** in the vessels with different diameter; ns – non-significant (ANOVA followed by Tukey's multiple comparison test). **C-D.** Quantification of micro- **(C)** and macroleakages **(D)** occurred on different distance to tumor cells. For consistency *p* values are shown for the same pairs as on Figure 6D-F; ns – non-significant (ANOVA followed by Tukey's multiple comparison test). **E.** Percentage of neutrophil-infiltrated vessels on different distance to tumor cells.

Figure S15. Identification of leaky vessel type.

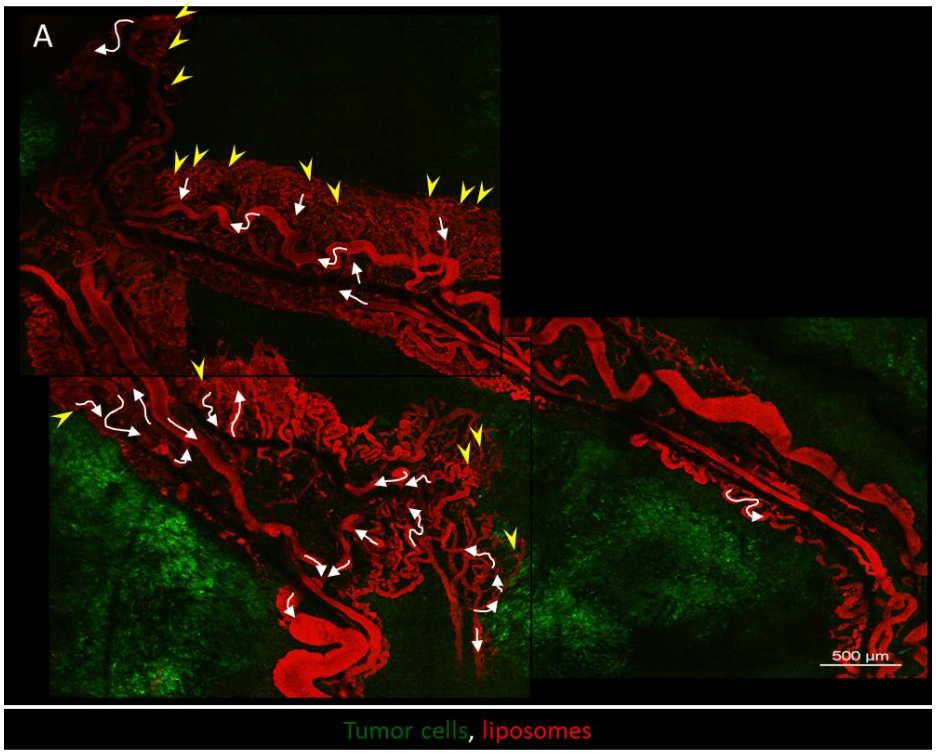

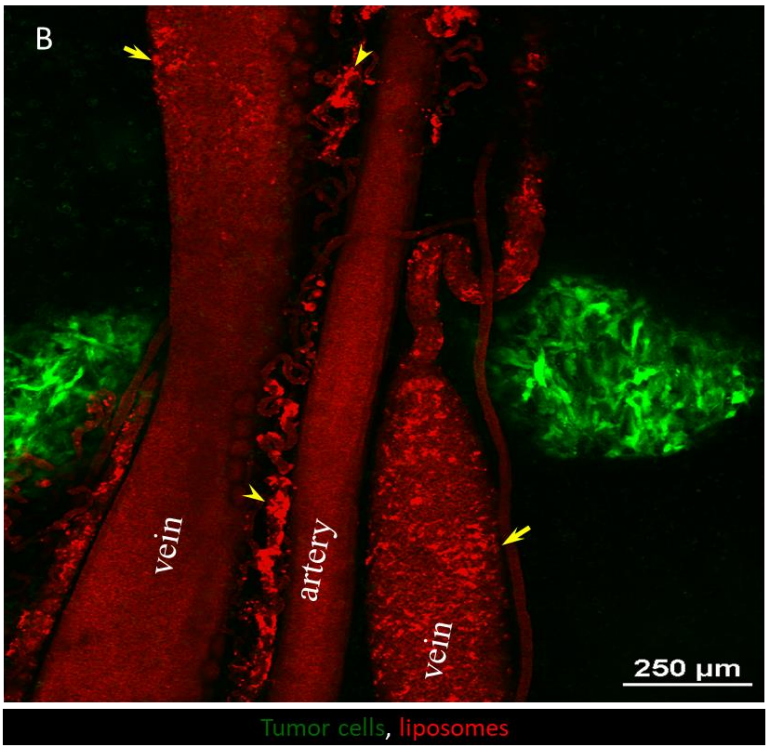

A. Vast area of B16 tumor was reconstructed and resonant scanner was used to identify blood flow direction in individual vessels (white arrows) for differentiation between afferent and efferent vasculature. Leakage spots (yellow arrowheads) were found mainly in efferent vessels. **B.** Representative image of tumor-supplying artery and two tumor-draining veins in B16 tumors identified by morphology and blood flow rate. Multiple leakage spots were found in veins (arrows) and venules (arrowheads), but not in arteries.

Figure S16. Analysis of vessel specific determinants for liposomes extravasation.

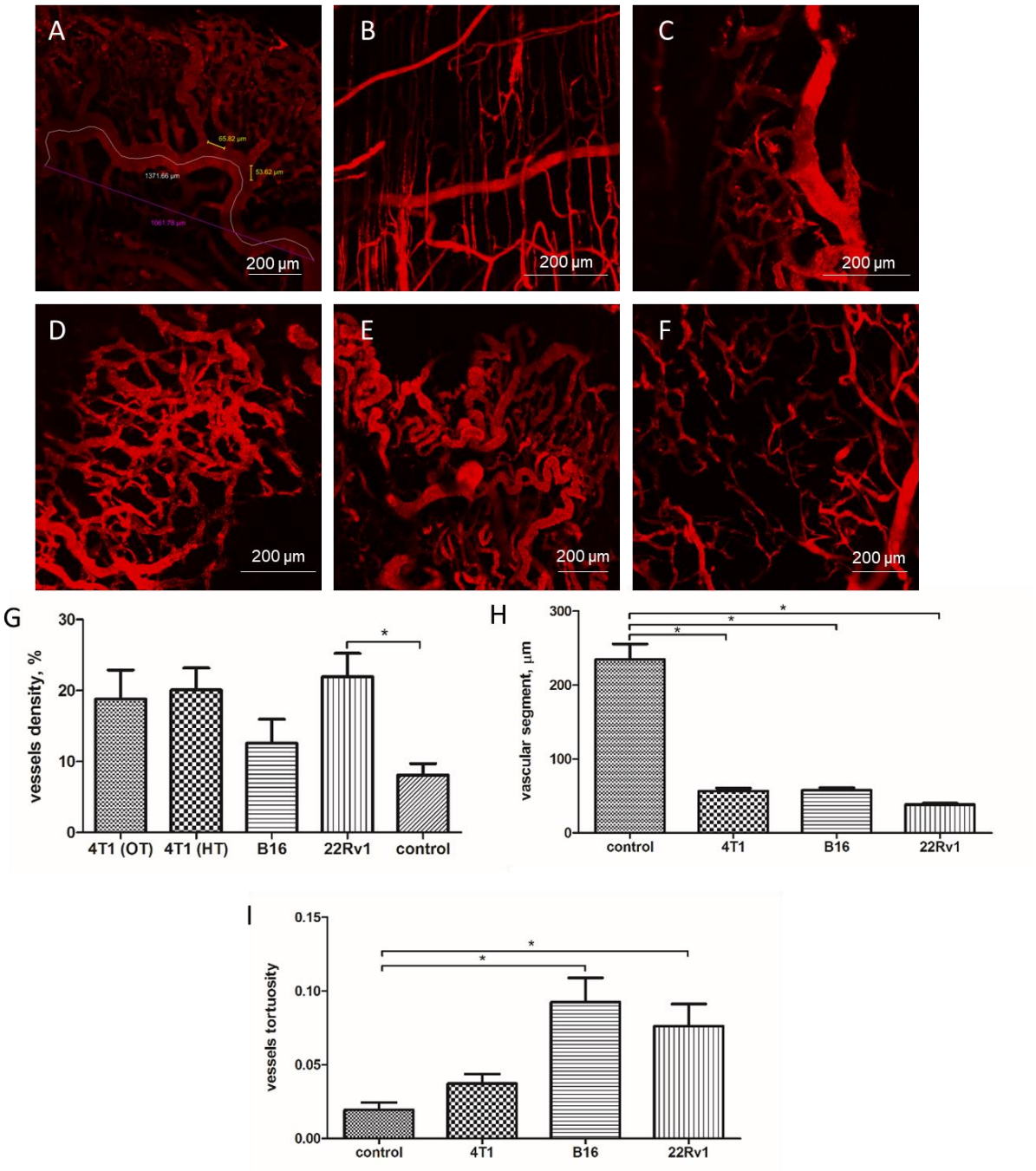

A. Example of vascular segment and tortuosity measurement. Vascular segment is identified as distance between two adjacent branches (yellow lines). Tortuosity (T) is defined *via* vascular path (VP) between two points (white line) and the geometric distance (GD) between those points (magenta) using the equation T=(VP-GD)/VP. **B-F.** Representative IVM images of the control vessels in healthy skin **(B)**, 4T1 orthotopic **(C)** and heterotopic **(D)** models, B16 **(E)** and 22Rv1 **(F)** tumors. **G.** Quantification of overall vessels density in tumor models. **H.** Quantification of vascular segment in tumor models. **I.** Quantification of tortuosity index in tumor models. *p<0.05 (ANOVA followed by Tukey's multiple comparison test).

Figure S17. Measurements of selected tumor characteristics.

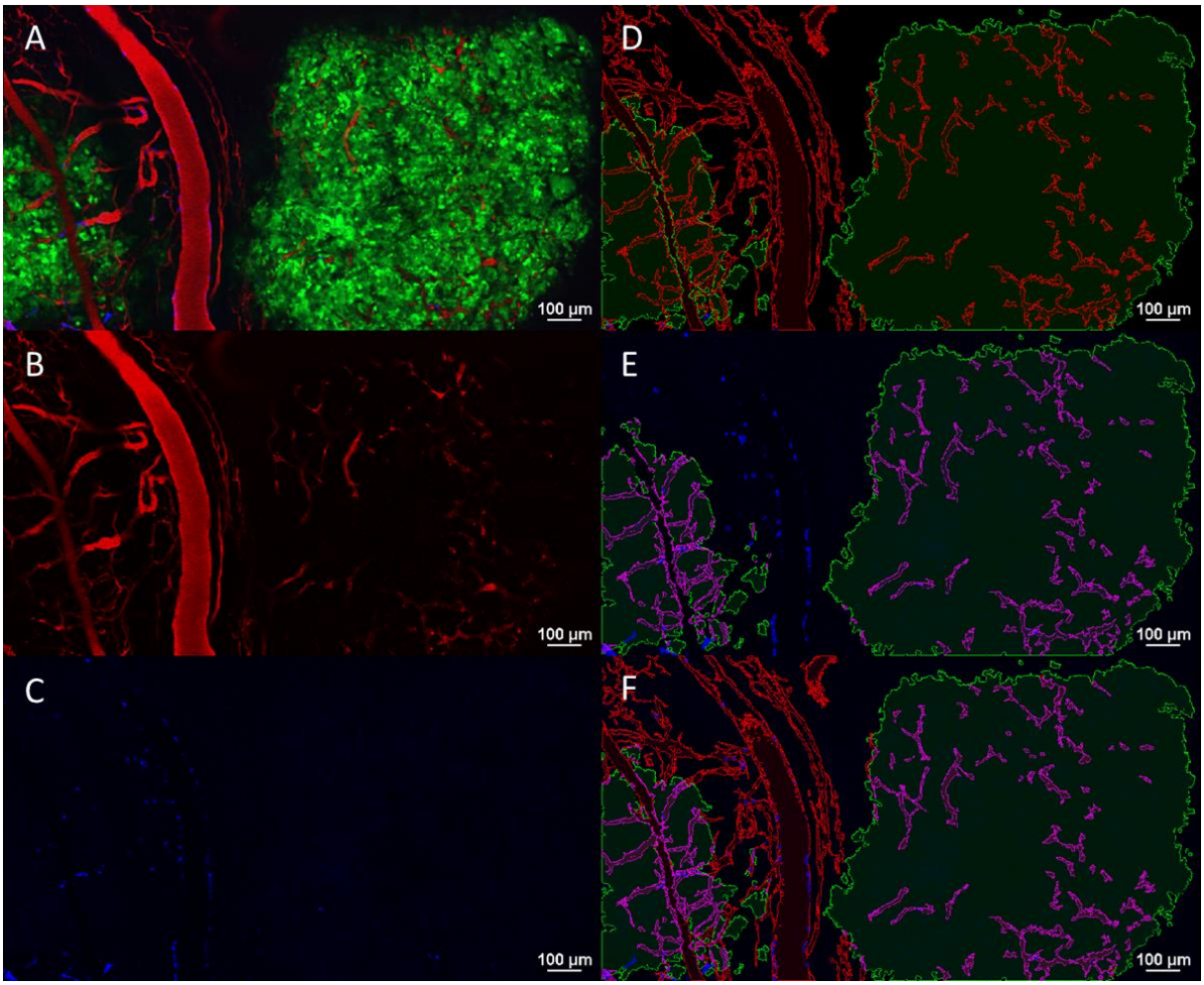

A. Representative IVM image of tumor microenvironment demonstrating tumor cells (green), vessels counterstained by circulating FL (red) and neutrophils (blue). **B** and **C** represent separate channels from **A** for tumor vasculature and neutrophils, respectively. **D**. Using NIS Elements AR software green and red masks are generated to depict tumor area and vessels area, respectively. **E**. Intersection between green and red masks (shown in magenta) is used to delineate intratumoral vasculature. Blue mask depicts total neutrophils area. **F**. Resulted image includes masks for tumor (green), intratumoral (magenta) and peritumoral (red) vasculature, and neutrophils (blue), that are used for automatic area measurements.

Figure S18. Analysis of leukocytes population and liposomes capturing in 4T1 tumor.

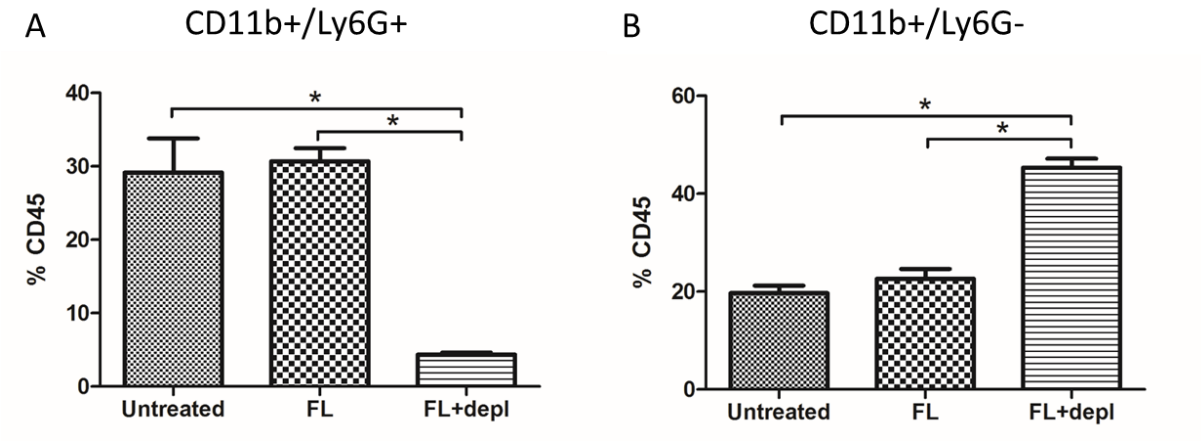

A-B. Neutrophils **(A)** and macrophages/dendritic cells **(B)** counts are shown as percentage of CD45+ cells in 4T1 tumors of untreated mice (n=4), FL-treated (n=6) and Ly6G-depleted 24 h prior to FL injection (n=6); *$p<0.05$ (ANOVA followed by Tukey's multiple comparison test).

Figure S19. Flow cytometry gating strategy for analysis of subtumoral compartments and liposomes cellular uptake.

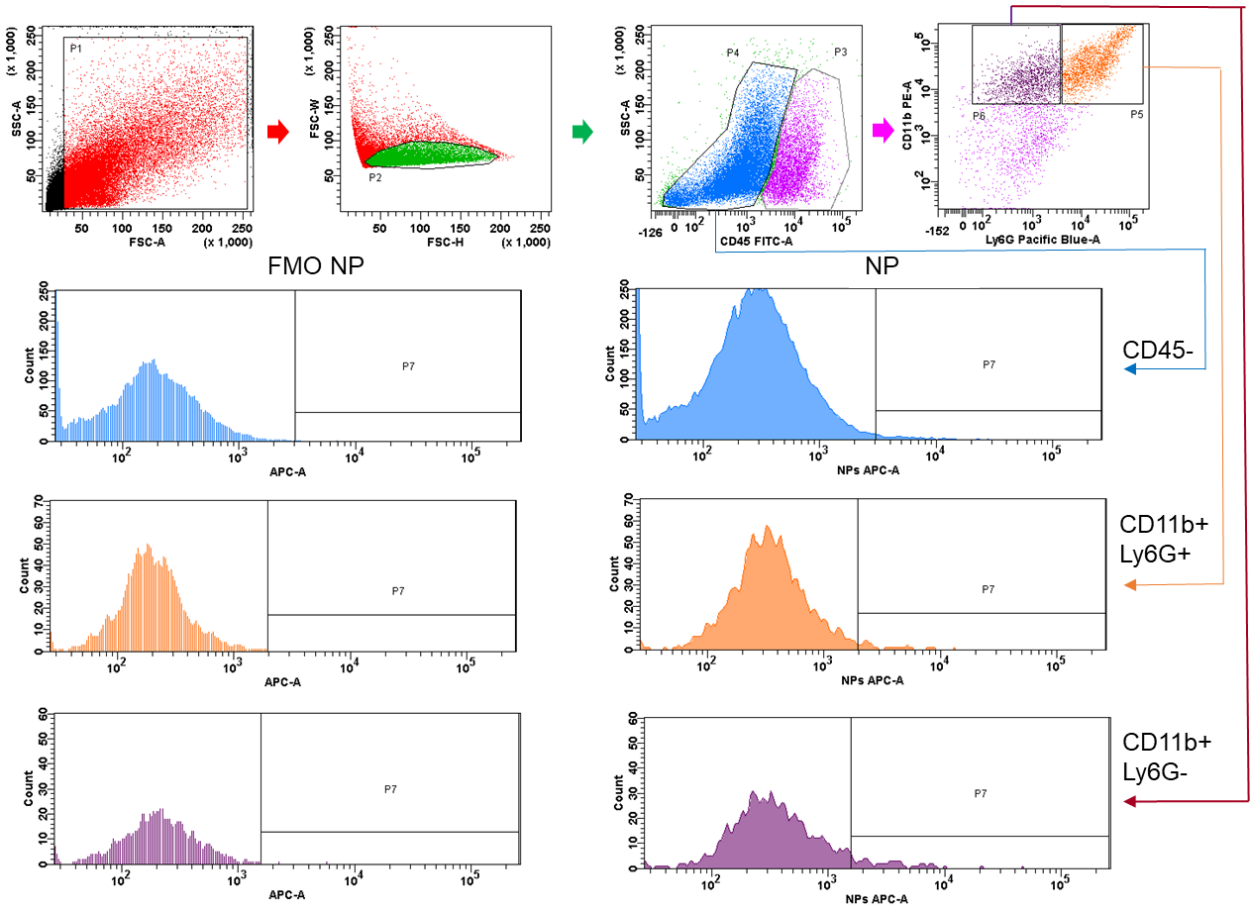

After excluding cell debris and duplets from analysis based on forward and side light scatter characteristics cells were divided into CD45- (non-leukocytes) and CD45+ (leukocytes) populations and from the latter CD11b+Ly6G+ (neutrophils) and CD11b+Ly6G- (macrophages/dendritic cells) subpopulations were gated. Next, FL signal distribution in APC fluorescence channel was plotted on histograms in selected cells subpopulations. Linear gates were set to discriminate positive events (right) based on respective FL fluorescence minus one (FMO) controls for each subpopulation (left) and FL cellular uptake was quantified.

Figure S20. Liposomes accumulation in 4T1 tumors upon Gr1 depletion.

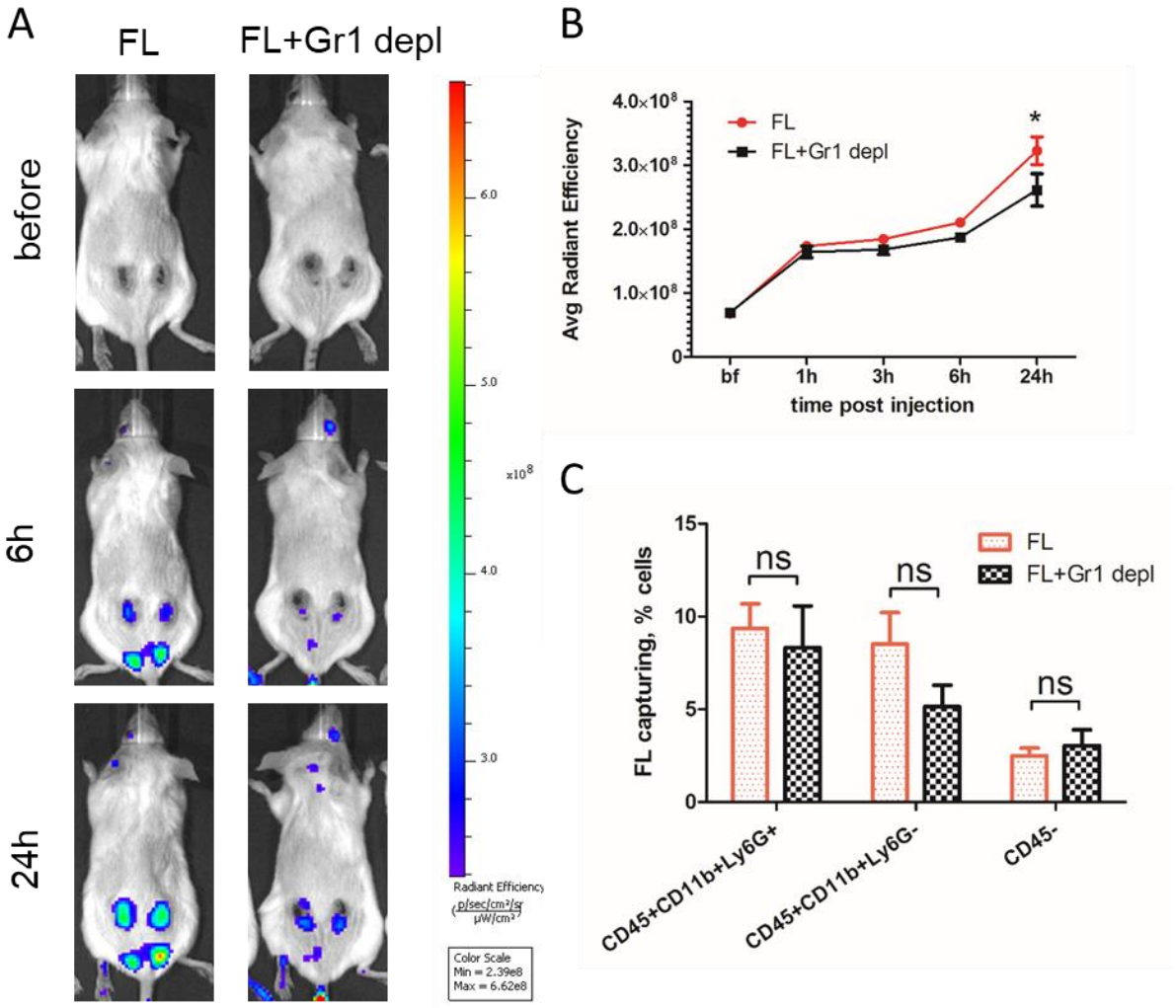

A. Representative images of FL accumulation in bilateral 4T1 tumors after i.v. injection in control (FL) and anti-Gr1 antibodies treated (FL+Gr1 depl) mice. Depleting antibodies were injected i.p. (250 µg/mouse) 24h prior to FL treatment. **B.** Quantification of mean fluorescence intensity from tumors in untreated (n=6) and Gr1-treated mice (n=4); *$p<0.05$ (ANOVA followed by Bonferroni multiple comparison test). **C.** Quantification of liposomes capturing in 4T1 tumors with and without Gr1 depletion by flow cytometry 24h after FL injection (for gating strategy see Figure S19); ns – non-significant (unpaired t-test).

Supplementary Videos

Supplementary Video 1. Liposomes extravasation through microleakage (arrows).

Supplementary Video 2. Liposomes extravasation through macroleakage (arrows).

Supplementary Video 3. IVM of pulsing macroleakage. Tumor vessel imaging (left frame) immediately after FL (25 mg/kg lipids) i.v. injection and fluorescence intensity measurements (right frame) in the vessel (green) and interstitial space inside (yellow) and outside (magenta) macroleakage area. Arrows indicate three subsequent waves of liposomes extravasation.

Supplementary Video 4. IVM of tumor-free skin at the time of FL i.v. injection (25 mg/kg lipids); microleakage spots are indicated by arrows; red, liposomes.

Supplementary Video 5. IVM of 4T1 orthotopic tumors at the time of FL i.v. injection (25 mg/kg lipids); microleakages (1st video) and macroleakage (2nd video) are indicated by arrows; red, liposomes; green, tumor cells.

Supplementary Video 6. IVM of 4T1 heterotopic tumors at the time of FL i.v. injection (25 mg/kg lipids); microleakages (1st video) and macroleakage (2nd video) are indicated by arrows; red, liposomes; green, tumor cells.

Supplementary Video 7. IVM of B16 tumors at the time of FL i.v. injection (25 mg/kg lipids); microleakages (1st video) and macroleakage (2nd video) are indicated by arrows; red, liposomes; green, tumor cells.

Supplementary Video 8. IVM of 22Rv1 tumors at the time of FL i.v. injection (25 mg/kg lipids); microleakage spots are indicated by arrows; red, liposomes; green, tumor cells.

Supplementary Video 9. Tracking for monocytes in tumor microenvironment 30 min after FL i.v. injection (25 mg/kg lipids); after capturing FL monocytes demonstrate either crawling (1st video) or stationary (2nd video) behavior; red, liposomes; green, Ly6G; blue, CD11b.

Supplementary Video 10. Neutrophil extravasation followed by microleakage development (arrow); red, liposomes; green, Ly6G.

Supplementary Video 11. Neutrophil extravasation followed by macroleakage development (arrow); red, liposomes; green, Ly6G.